XI International Conference on Computational Plasticity. Fundamentals and Applications
COMPLAS XI
E. Oñate and D.R.J. Owen (Eds)

TOWARDS A NUMERICAL SIMULATION OF DIRECT MANUFACTURING OF THERMOPLASTIC PARTS BY POWDER LASER SINTERING
COMPLAS XI

D. DEFAUCHY[1], G. REGNIER[1], I. AMRAN[1], P. PEYRE[1]
A. AMMAR[2] AND F. CHINESTA[3]

[1] Arts et Métiers ParisTech, PIMM, CNRS
151 Boulevard de l'Hôpital, Paris France
e-mail: denis.defauchy@ensam.eu, http://pimm.paris.ensam.fr

[2] Arts et Métiers ParisTech, LAMPA
2 boulevard du Ronceray, Angers, France
e-mail: amine.ammar@ensam.eu

[3] EADS Corporate International Chair
Ecole Centrale de Nantes, 1 rue de la Noë, Nantes, France
e-mail: francisco.chinesta@ec-nantes.fr

Key words: Coalescence, Thermoplastic powder, C-NEM, Selective Laser Sintering (SLS), Simulation.

Abstract. Direct manufacturing technology using Selective Laser Sintering (SLS) on thermoplastic powders allows obtaining final parts in a short time, with classical polymer density and a high flexibility of shape and evolution of parts. The physical base of this process is the coalescence of grains, which initiates the densification of powder during SLS. This study presents a 2D C-NEM simulation of the whole process. We firstly focus on the chosen method and its advantages. We present the simulation details and validate the modeling through a 2D infinite cylinders coalescence simulation. The mesh of the grain interface is continuously adapted to the local curvature to better capture the coalescence phenomenon. We are able to simulate the sintering of twelve particles laying on a support within some hours.

1 INTRODUCTION

1.1 Selective laser sintering process

Polymer Parts obtained by direct manufacturing with laser sintering technology present porosities [1] which significantly reduce their mechanical resistance [2]. This porosity is due to the air between polymer powder grains which remains trapped into the material while polymer is melting. As the process needs to be performed with temperature variations, air

volume evolutions have to be taken into account, influencing directly the density of the material. It is also important to be able to predict the conditions in which porosity volume will be minimal.

The important material parameters acting in the process are the viscosity, the surface tension and the laser absortivity of the polymer.

Parts manufacturing by SLS is difficult for some reasons. Firstly, the polymer powder degrades while performed in the machines [3] maintained at high temperatures for some hours. It is also difficult to predict the polymer solidification, which depends on the cooling conditions as semicrystalline polymers are mainly used [4].

Among all articles cited here, it appears that the main controllable process parameters influencing the final material can be classed in order of importance [5]: layer thickness, laser speed, pre-heating powder bed temperature and laser power (most important). Some of these results have been confirmed through a finite element model [6]. Some other parameters are discussed as laser beam diameter, hatch distance and layering conditions. It seems clear that the use of a CO2 laser (10.6 μm) to melt the polymer powder is recommended.

All these parameters are often connected. For example, when particle size is decreased, the layering becomes difficult [4]. Among all articles cited here, studies concerning the influence of each process parameters and their relation on the final material can be found.

In parallel to the experiences, it is important to simulate the process for a better understanding of the parts characteristics. Simulating the process will enable to choose the best parameters for the manufacturing and predict the performances of SLS polymer parts, and as soon as the simulation is functional, have this information faster.

1.2 Physics of coalescence

The first coalescence model has been made by Frenkel [7] and improved a few years later by Eshelby [8]. Describing the evolution of the coalescence with three parameters (Figure 1), the neck radius y, the particles radius a, and the angle θ, they could quite well predict the evolution of the coalescence phenomenon in time (Equation 1) .

$$\frac{y}{a} = sin\left(\tau^{\frac{1}{2}}\right) \tag{1}$$

They could show that the coalescence is driven by the surface tension Γ while the viscosity η and the initial particles radius a_0 slow the phenomenon, introducing a dimensionless time τ (Equation 2).

$$\tau = \frac{t\Gamma}{\eta a_0} \tag{2}$$

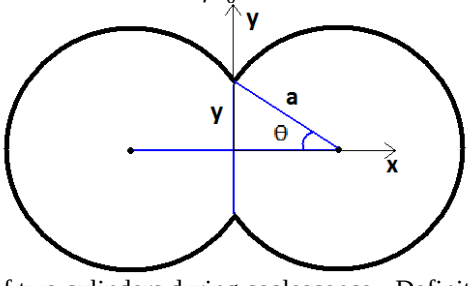

Figure 1: Shape of two cylinders during coalescence - Definition of parameters.

Other works have been done later [9,10] by taking into account a viscoelastic behaviour for

the polymer.

The presence of numerous necks on a particle induces effects in the kinetics of coalescence. It has been shown experimentally that the arrangement of particles has an effect on the coalescence rate [11].

1.3 Coalescence simulations

Finite element simulations of capillary driven flows have been done to evaluate the influence of grain sizes and several growing necks on particles.

One of the first finite element simulations [12] from 1995 is based on axisymmetric isothermal assumptions and shows the influence of multiples aligned particles in the coalescence phenomenon.

The first 3D finite element simulation of complicated initial geometries [13] confirmed the necessity to go further to understand the sintering of particles. In parallel to the previous study, authors presented [14] very well numerical difficulties like mesh distortions for large deformations (fluids) and front tracking methods. These methods are very useful in the cases of capillary flows to well describe the interface but can induce border inaccuracy and wrong surface tension evaluation. Furthermore, sintering problems seems to induce difficulties in convergence of iterative methods due to the matrix form and the mesh distortion increases these difficulties, then, it is necessary to remesh the domain. However, it is difficult to remesh a border which has no analytical definition.

Rotomolding process presents similarities to SLS. Main differences are the heating conditions, the polymer in SLS process melted by the laser action, from the free side of the powder layer. A study presents a isothermal simulation of the densification of spheres [15] trying to characterize the evolution of the air trapped into the material. The size of particles and rheology of material influence the bubbles size and the air trapped into cavities is supposed to diffuse through the polymer after the closure of cavities.

Finally, studies [16,17,18] show that the polymer viscoelasticity has an influence at the early stage of coalescence. Globally, the elasticity influence seems not to have a strong effect on the coalescence rate.

1.4 Objectives

The aim of this work is to simulate the SLS process in 2D to study the coalescence of a significant set of grains and to be able to know if the simulation can be extended to the 3D.

We first present all the details of our computation and results. To validate the modelling, we simulate the isothermal coalescence of two same size particles and compare it to a 2D coalescence model based on Frenkel-Eshelby 3D one. Then the coalescence of a set of grains is simulated in anisothermal conditions.

2 MODELLING LASER SINTERING

2.1 C-NEM Simulation

The C-NEM method [19,20] (Constrained Natural Element Method) is mainly based on usual Voronoï cells around nodes. The main advantage of this method is to take into account, in streams interpolations, the participation of all nearest neighbours around a point on the

domain. As a consequence, the mesh is not constrained as it is in a current finite element method (FEM). Performing FEM, it is important to have no distorted elements in the mesh. The remeshing of the whole domain is frequently needed, which is computer time consuming. In a C-NEM computation, the nodes can move without any problem and is also well adapted for process simulations, as the domains have often large deformations.

The C-NEM method used here is defined by the fact that the velocity is interpolated by constrained Sibson natural element shape functions φ while the pressure P is assumed constant by cell interpolated by the shape functions ψ. The weak formulation integration is done by nodal integration and the velocity gradient is done using the SCNI method (Stabilized Conform Modal Integration).

Taking this into account, the problem is discretized and the velocity u, pressure p and temperature T expressions are developed (Equations 3,4,5) with their nodal values.

$$u(x,y) = \sum_{i=1}^{Nd} \varphi_i \begin{pmatrix} Ui \\ Vi \end{pmatrix} = N^T U = \begin{pmatrix} \varphi_1 & 0 & \dots & \varphi_k & 0 & \dots & \varphi_N & 0 \\ 0 & \varphi_1 & \dots & 0 & \varphi_k & \dots & 0 & \varphi_N \end{pmatrix} \begin{pmatrix} U_1 \\ V_1 \\ \vdots \\ U_k \\ V_k \\ \vdots \\ U_N \\ V_N \end{pmatrix} \tag{3}$$

$$p(x,y) = \sum_{i=1}^{Nd} \psi_i P_i = \bar{N}^T P = \begin{pmatrix} \psi_1 & \dots & \psi_k & \dots & \psi_N \end{pmatrix} \begin{pmatrix} P_1 \\ \vdots \\ P_k \\ \vdots \\ P_N \end{pmatrix} \tag{4}$$

$$T(x,y) = \sum_{i=1}^{Nd} \varphi_i T_i = N^T \bar{T} = \begin{pmatrix} \varphi_1 & \dots & \varphi_k & \dots & \varphi_N \end{pmatrix} \begin{pmatrix} T_1 \\ \vdots \\ T_k \\ \vdots \\ T_N \end{pmatrix} \tag{5}$$

where x and y are the coordinates on the domain, U_i and V_i the nodal velocities on $\vec{x}$ and $\vec{y}$, T_i the nodal temperature, φ_i and ψ_i the nodal shape functions and Nd the number of nodes.

2.2 Basic equations

In high viscosities capillarity flows, velocities are very small, then inertial terms can be neglected and the polymer can be considered as a Newtonian viscous fluid.

The basic equations which drives the fluid movements are given (the local equilibrium - Equation 6) using the deformation tensor D (Equation 7).

$$\begin{cases} \nabla . \sigma + f_d = 0 \\ \sigma = -pI + 2\mu D \\ \nabla . V = 0 \end{cases} \tag{6}$$

where σ is the strain tensor, fd the volume force in the domain, D the deformation tensor and μ the viscosity.

$$D = \begin{pmatrix} \dfrac{\partial u}{\partial x} & \dfrac{1}{2}\left(\dfrac{\partial u}{\partial y} + \dfrac{\partial v}{\partial x}\right) \\ \dfrac{1}{2}\left(\dfrac{\partial u}{\partial y} + \dfrac{\partial v}{\partial x}\right) & \dfrac{\partial v}{\partial y} \end{pmatrix} \tag{7}$$

2.3 Computation of equations on the discretized domain

The basic equations are integrated on the domain introducing the variational formulation (Equation 8,9) depending on the vectors U and P.

$$U^{*T}\left[\int_{\Omega} 2\mu B^T B\, d\Omega\right]U - U^{*T}\left[\int_{\Omega} B^T \tilde{I}\overline{N}^T\, d\Omega\right]P - U^{*T}\left[\int_{\partial\Omega} N(\Gamma\kappa - P)n\, dS + \int_{\Omega} N f_d\, d\Omega\right] = 0$$

$$\tilde{I} = \begin{bmatrix}1\\1\\0\end{bmatrix}, B = \begin{pmatrix} \varphi_{1,x} & 0 & \cdots & \varphi_{k,x} & 0 & \cdots & \varphi_{N,x} & 0 \\ 0 & \varphi_{1,y} & \cdots & 0 & \varphi_{k,y} & \cdots & 0 & \varphi_{N,y} \\ \frac{\varphi_{1,y}}{\sqrt{2}} & \frac{\varphi_{1,x}}{\sqrt{2}} & \cdots & \frac{\varphi_{k,y}}{\sqrt{2}} & \frac{\varphi_{k,x}}{\sqrt{2}} & \cdots & \frac{\varphi_{N,y}}{\sqrt{2}} & \frac{\varphi_{N,x}}{\sqrt{2}} \end{pmatrix} \tag{8}$$

where κ is the local curvature and n the normal vector on the surface.

$$U^T\left[\int_{\Omega} B^T \tilde{I}\overline{N}^T\, d\Omega\right]P^* = 0 \tag{9}$$

By introducing the vector $\overline{U}$ (Equation 10) which enables to regroup all the degrees of freedom in one vector, the system can be defined with one matrix (Equation 11).

$$\overline{U} = \begin{pmatrix} U_1 \\ V_1 \\ P_1 \\ \vdots \\ U_N \\ V_N \\ P_N \end{pmatrix} \tag{10}$$

$$\overline{U}^{*T} K \overline{U} - \overline{U}^{*T} F = 0 \tag{11}$$

Details on the matrix K and the vector F are given in Equations 12 and 13.

$$K_{ij} = \int_{\Omega} \begin{pmatrix} 2\mu\left(\varphi_{i,x}\varphi_{j,x} + \frac{\varphi_{i,y}\varphi_{j,y}}{2}\right) & \mu\varphi_{i,y}\varphi_{j,x} & -\varphi_{i,x}\psi_j \\ \mu\varphi_{i,x}\varphi_{j,y} & 2\mu\left(\varphi_{i,y}\varphi_{j,y} + \frac{\varphi_{i,x}\varphi_{j,x}}{2}\right) & -\varphi_{i,y}\psi_j \\ -\varphi_{j,x}\psi_i & -\varphi_{j,y}\psi_i & 0 \end{pmatrix} \tag{12}$$

$$F = \int_{\Omega} \begin{pmatrix} \varphi_1 & 0 \\ 0 & \varphi_1 \\ 0 & 0 \\ \vdots & \vdots \\ \varphi_k & 0 \\ 0 & \varphi_k \\ 0 & 0 \\ \vdots & \vdots \\ \varphi_N & 0 \\ 0 & \varphi_N \\ 0 & 0 \end{pmatrix} \rho\begin{pmatrix} f_x \\ f_y \end{pmatrix} d\Omega + \int_{\partial\Omega} \left(\frac{\Gamma}{R} - P\right) \begin{pmatrix} \varphi_1 & 0 \\ 0 & \varphi_1 \\ 0 & 0 \\ \vdots & \vdots \\ \varphi_k & 0 \\ 0 & \varphi_k \\ 0 & 0 \\ \vdots & \vdots \\ \varphi_N & 0 \\ 0 & \varphi_N \\ 0 & 0 \end{pmatrix} \begin{pmatrix} n_x \\ n_y \end{pmatrix} dS \tag{13}$$

2.4 Displacement boundary limit conditions

During SLS simulation, the displacement boundary limit conditions will be set by representing the true limit conditions of the powder tray. The three rigid body displacements are blocked.

However, to be able to simulate the coalescence of particles with no displacement boundary limit conditions, three Lagrangian conditions (Equations 14,15,16) are added in the

system, Equation 11 is used to block the 3 rigid body movements.

The two translations on x and y are blocked through a global condition on the displacement of the domain, which has to be null (Equations 14,15).

$$\sum Vol_i U_i = 0 \tag{14}$$

$$\sum Vol_i V_i = 0 \tag{15}$$

where Vol_i is the Voronoï cell area in 2D, around node i.

The z rotation is blocked through a global condition on the rotation of the domain (Equation 16).

$$\sum_{i=1}^{Nd} \frac{\left|\underline{u_i}.(\underline{z}\Lambda\underline{GM_i})\right|}{\left\|\underline{GM_i}\right\|^2} = 0 \tag{16}$$

where G is the gravity center of the domain, which remains constant during the coalescence, u_i the velocity of the node M_i.

As fluids are considered, the global conditions on all nodes are needed to not deform the domain.

2.5 Time step calculation

While simulating coalescence, a too large time step induces small inaccurate local curvatures on the border. This induces bad movements which influence the rest of the simulation.

The time step is also constrained with movements, by limiting the local rotation of the two segments joining each node of the border to an angle value of some degrees.

2.6 Cavities (Volume, Pressure)

At the beginning, the pressure was set on the border of the domain. The air in the cavities was assumed compressible and cavities presented oscillating volume variations. To avoid these problems, the only solution was to strongly decrease the time step

Simulating the sintering of a Polyamide 12 of about 1000 Pa.s of viscosity, no significant pressure variations were observed in cavities. The pressure will also be assumed constant.

We decided to use the perfect gas law, calculating the cavities volumes at each time step according to the temperature variation.

Knowing the theoretical volume of the cavity, a Lagrangian condition is created in the system (Equation 17) for each cavity, imposing its derivative.

$$\frac{\mathrm{dVol}}{\mathrm{dt}} = \frac{1}{2}\sum_{\mathrm{i=1}}^{\mathrm{Nd}} \left[\begin{pmatrix}\mathrm{U_i}\\ \mathrm{V_i}\end{pmatrix} \Lambda \begin{pmatrix}\mathrm{x_{i+1}}\\ \mathrm{y_{i+1}}\end{pmatrix} - \begin{pmatrix}\mathrm{U_{i+1}}\\ \mathrm{V_{i+1}}\end{pmatrix} \Lambda \begin{pmatrix}\mathrm{x_i}\\ \mathrm{y_i}\end{pmatrix}\right] \tag{17}$$

$$i+1 = 1 \; if \; i = N$$

where x_i and y_i are the components of the velocity of the node i.

As the time step is linked to the velocity of the nodes, it is not determined before the resolution of the system and the time step is chosen as the maximum value on some precedent time steps to avoid node oscillations.

2.7 Mesh

Node density should not be important except on the border of the domain to well take into

account the surface tension. The initial mesh is indeed adapted to the curvature on the border, nodes are created and deleted depending on the local curvature during the simulation.

2.8 Surface tension modeling

The surface tension effect (Equation 18) has to be discretized.

$$F_{tension} = \int_{\partial\Omega} N \frac{\Gamma}{R} n \, dS \tag{18}$$

The nodal curvature is determined by the radius of the circle passing by the considered node and its two neighbors (Figure 2).

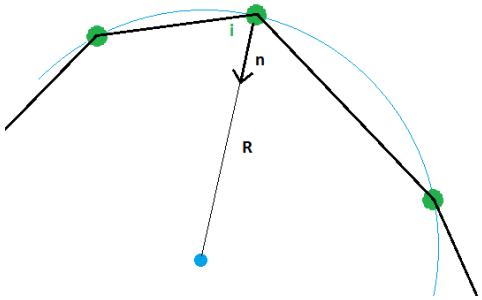

Figure 2: Surface tension calculation on discretized domain

2.9 Numerical details

The system to solve (Equation 19) presents three degrees of freedom per node (U,V,P).

$$KU = F, U = (U\ V\ P\ \dots) \tag{19}$$

The iterative methods GMRES and PCG were used but it was difficult to get the convergence. We separate the pressure and the velocity (Equation 20,21), and add a compressible coefficient of 10^6 Pa.s into the matrix C to keep the quasi-incompressible behavior of the polymer.

$$\begin{pmatrix} A & B \\ B^T & C \end{pmatrix} \begin{pmatrix} U \\ P \end{pmatrix} = \begin{pmatrix} F \\ G \end{pmatrix} \tag{20}$$

$$\begin{cases} AU + BP = F \\ B^T U + CP = G \end{cases} \rightarrow P = C^{-1}G - C^{-1}B^T U \rightarrow AU + BC^{-1}G - BC^{-1}B^T U = F \tag{21}$$

The system obtained has a length of 66% of the initial one (Equation 22) and iterative methods converge well to the solution.

$$(A - BC^{-1}B^T)U = F - BC^{-1}G \tag{22}$$

This method gives the same results than considering that the polymer is compressible in the local equilibrium equations.

The displacements of the nodes are calculated through a Taylor development at second order (Equation 23) by calculating the acceleration on two time steps (Equation 24).

$$X(t + dt) = x(t) + v(t)dt + \gamma(t)\frac{dt^2}{2} \tag{23}$$

$$\gamma(t) = \frac{v(t) - v(t - dt)}{dt} \tag{24}$$

2.10 Heating conditions

SLS process is performed in a complex transient thermal situation. The temperature is set on the stage and the vertical sides (Figure 3). Air convection at the upper surface of the polymer is modelled by a heat exchange coefficient. The laser heats the material during its

Laser

pass. The polymer coalescence is considered in the studied area.

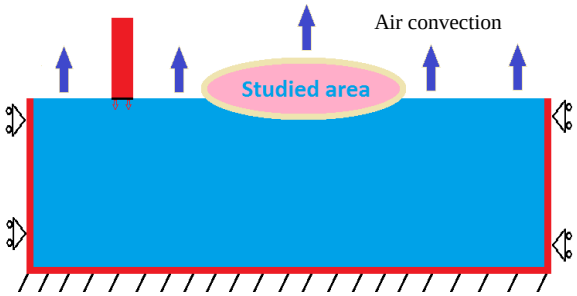

Figure 3: Thermal and displacement limit conditions of the simulation

The cavities are supposed not to exchange energy, and their temperatures are calculated by a mean calculation on their surface and nodal temperatures. Their temperature changes induce volume changes, pressure assumed constant (Section 2.6).

The viscosity, which is dependent on the temperature, is applied through an Arrhenius law (Equation 25), and its maximum value (solid material) is limited with a high viscosity of 10.000 Pa.s, which seems to be enough to limit coalescence.

$$\mu(T) = Ke^{\frac{E}{RT}} \tag{25}$$

As done for the mechanical behaviour of the polymer (U,V,P), a thermal numerical resolution of the temperature of the domain is performed beginning with the local equilibrium equation (Equation 26).

$$\lambda \Delta T + P = \rho c \frac{\partial T}{\partial t} \tag{26}$$

where λ is the thermal conductivity, P the heat source, ρ the volume mass and c the heat capacity

By introducing three parameters (Equation 27), and performing a variational formulation on the domain, the system to solve and its details are obtained (Equation 28 & 29):

$$\begin{aligned} b &= \frac{P}{\rho c} \\ k &= \frac{\lambda}{\rho c} \\ \varphi &= -\lambda \nabla \mathrm{T} \end{aligned} \tag{27}$$

$$\underline{\underline{M}}\dot{\bar{T}} = -\underline{\underline{K}}\,\bar{T} + \underline{B} \tag{28}$$

$$\begin{aligned} \underline{\underline{K}} &= k \int_{\Omega} \frac{\partial N}{\partial \underline{x}} \frac{\partial N^T}{\partial \underline{x}} \, d\Omega \\ \underline{B} &= -\frac{1}{\rho c} \int_{\partial\Omega} N\varphi.n \; d\Gamma + \int_{\Omega} Nb \, d\Omega \\ \underline{\underline{M}} &= \int_{\Omega} NN^T \, d\Omega \\ \dot{\bar{T}} &= \frac{\partial \bar{T}}{\partial t} \end{aligned} \tag{29}$$

Evaluating the derivative of temperature with time by a Taylor development at order 1 (Equation 30), the new nodal temperature (Equation 31) is calculated by an implicit method.

$$\dot{\bar{T}}^n = \frac{\bar{T}^{n+1} - \bar{T}^n}{\Delta t} \tag{30}$$

$$\bar{T}^{n+1} = \left[\frac{\underline{\underline{M}}}{\Delta t} + \underline{\underline{K}}\right]^{-1} \left(\frac{\underline{\underline{M}} T^n}{\Delta t} + B\right) \tag{31}$$

2.11 Laser action

The first test was to set a volume action into the whole height of the polymer to validate the principles, and then a more realistic model has been employed by applying a Gaussian repartition of the power flux on the surface [21].

It was necessary to find the nodes directly under laser beam (Figure 4).

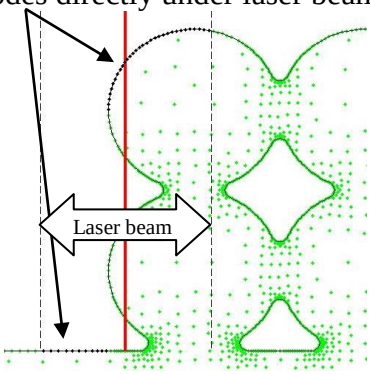

Figure 4: Nodes under laser action (Black)

The idea of the algorithm is the following. Working on the free surface of the domain, nodes are considered from the left to the right. Firstly cut the whole top surface exposed on one part to the laser, in different sections, depending on the x displacements changes (left to right and right to left) and under the edges of the laser field. Then identify all sections likely to be exposed to laser (surface whose direction is from left to right). Among these sections, determine which of the nodes under the laser is the highest, and begin the work from the section containing this node. All the nodes which will be considered here are under direct laser action. To the left (respectively to the right), and until crossing the laser beam boundary, identify whether the laser boundary is on the section or not. If not, proceed to the next section considering respectively the first node of next section as the first node of the section which is on the left (respectively right) of the last one of the studied section, and repeat the same work on the new section until crossing the laser demarcation. Finally, consolidate all the sections made by more than one node and manage some details on the sections extreme nodes, depending on whether the sections go up or down.

The laser time steps are adapted and the possibility to interpose movements during the laser pass is considered.

3 SIMULATION RESULTS

The simulation is computed on Matlab. The functions which have to be rapid (hydrodynamic and rigid matrix creation) are function written in C language called in Matlab.

3.1 Two cylinders coalescence

The first simulation is performed on the isotherm coalescence of two infinite cylinders in

order to validate the simulation [22]. A 2D model has been developed and the coalescence parameters *y* and *a* have been defined on the simulation to try to represent as well as possible the model. Good agreements were found between the model and the simulation.

3.2 Process simulation

We finally simulated the process taking into account the parameters exposed in Table 1 on a Polyamine 12. Applying the laser action on a non heated domain (Figure 5), it is seen that the laser/material interaction conduces to very high temperatures (15000°C) and it has been confirmed on COMSOL. The laser power has also been decreased from 5 W (normal SLS power) to 5.10^{-7} W to obtain a more realistic increase of temperature under laser action of about 100 °C to 200°C. This decrease of power induces the necessity to heat the domain from the sides to melt the polymer and see an evolution of the melting.

Figure 5 Laser action on polymer

Table 1: Process simulation parameters

Process parameters	Value	Material parameters	Value
Initial polymer temperature	150 °C	Cylinders diameter	100 µm
Border temperature	350 °C	Polymer Thermal conductivity	0.25 $W.m^{-1}.K^{-1}$
Air temperature	150 °C	Polymer density	1100 $Kg.m^{-3}$
Exchange convection coefficient	13 $W.m^{-1}.k^{-1}$	Air density	1.2 $Kg.m^{-3}$
Laser power	5.10^{-7} W	Gravity	9.81 $m.s^{-2}$
Laser beam diameter	200 µm	Surface Tension	0.03 $N.m^{-1}$
Laser velocity	1 $m.s^{-1}$	Polymer heat capacity	1700 $J.Kg^{-1}.K^{-1}$
Laser reflectivity	4 %	Arrhenius K (PA 12)	$3.5*10^{-6}$
		Arrhenius E (PA 12)	75647

Our results are presented simulating the sintering of 12 particles of Polyamide 12 lying on a support (Figure 6). The domain is heated from the bottom and the sides. The heat exchange with the air occurs. After 5 seconds, the laser is passing from the left to the right very rapidly (some ms), and symmetric displacements conditions are applied on both sides.

The principles are validated and the calculation specificities are exposed in table 2. Depending on the chosen parameters, mesh and time step conditions particularly, the calculation time can be much different, but results may be inaccurate. The best parameters are difficult to find at this time and work must be done to choose them.

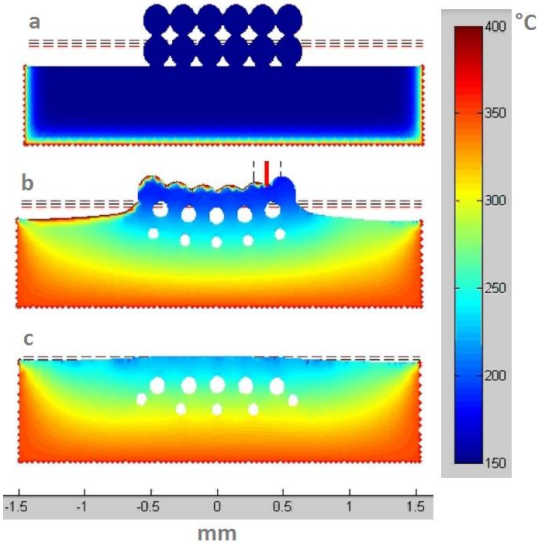

Figure 6: Captures of simulation evolution (a - solid polymer, b - laser pass, c - melted polymer) during the SLS process applied on 12 cylinders.

Furthermore, as the laser action is false and induces a high temperature on some local nodes, the movements become very high due to discontinuities and very low values of viscosities. This induces very small displacement time steps to limit local movements, which increase a lot the calculation time. The calculation presents 700 time step before laser pass (5s), 4500 time step during laser pass, and 2000 for the next 5 seconds. Without laser action, the same simulation gives a calculation time of 5.92 hours for 4362 time step.

Table 2: Calculation specificities for the presented simulation

Matlab	R2009B 64 bits	Nodes in final mesh	4381
Windows	7 64 bits	Number of movement time step	9067
RAM memory	DDR3 3*8 Go	Calculation duration	8.9 h
Processor	Intel Core i7-950	Laser pass calculation duration	0.57 h
Motherboard	ASUS P6T7	Volume conservation	100.0097 %

12 CONCLUSIONS

Selective laser sintering process is a complicated process in which thermal conditions are never the same for each layer. However, in chosen conditions, we are able to simulate the process in spite of the laser/material interaction, which has now to be improved.

At this time, the main difficulties consisted to obtain the iterative methods convergence, a well adapted mesh depending on the curvature, and the better choice on the time step to avoid to large mesh deformation inducing mesh distortions and next calculations.

After performing experiments with a CO_2 laser on polymer powder to characterize a Beer-Lambert law for the laser/material interaction, we will program it and begin simulations of multi grains conditions in 2D. In parallel, we will perform experiments on multi grains layers of polymer powders in a heat chamber to compare the simulation results with the experiments, and identify the multigrain influence on coalescence.

ACKNOWLEDGMENTS

This work is supported by the FUI Project FADIPLAST. The authors acknowledge all FADIPLAST partners for their enriching discussions.

REFERENCES

[1] G.V. Salmoria, J.L. Leite, R.A. Paggi, *Polymer Testing*, **28**, 746 (2009).
[2] M. Schmidt, D. Pohle, T. Rechtenwald, *CIRP Annals - Manufacturing Technology*, **56**, 205 (2007).
[3] D.T. Pham, K.D. Dotchev, W.A.Y. Yusoff, *Journal of Mechanical Engineering Science*, **222**, 2163 (2008).
[4] V.E. Beal, R.A. Paggi, G.V. Salmoria, A. Lago, *Journal of Applied Polymer Science*, **113**, 2910 (2009).
[5] P. Wang, X. Li, J. Xiao, F. Zhu, Y. Yang, *ICALEO 2006 - 25th International Congress on Applications of Laser and Electro-Optics, Congress Proceedings*, art. 517 (2006).
[6] L. Dong, A. Makradi, S. Ahzi, Y. Remond, *Journal of Materials Processing Technology*, **209**, 700 (2009)
[7] Frenkel J., *J. PhysNature,* **9**, 385 (1945).
[8] Pokluda O., Bellehumeur C.T., Vlachopoulos J., *AIChE Journal*, **43**, 3253 (1997).
[9] Bellehumeur C.T., Kontopoulou M., Vlachopoulos J., *Rheologica Acta*, **37**, 270 (1998).
[10] Eshelby J. D., *Metallurgical Transactions*, **185**, 796 (1949).
[11] Asgapour M., Bakir F., Khelladi S., Khavandi A., Tcharkhtchi A., *Journal of Applied Polymer Science*, **119,** 2784
[12] Martinez-Herrera J. I., Derby J. J., *American Ceramic Society*, **78**, 645
[13] Zhou H., Derby J., *Theory and Modeling of Glasses and Ceramics*, **81**, 533
[14] Zhou H., Derby J., *International Journal for Numerical Methods in Fluids*, **36**, 841
[15] Bellehumeur C. T., Tiang J. S., *Polymer Engineering and Science*, **42**, 215 (2002).
[16] Lin Y. Y., Hui C. Y., Jagota A., *Journal of Colloid and Interface Science*, **237**, 267 (2001).
[17] Scribben E., Baird D., Wapperom P., *Rheological Acta*, **45**, 825 (2006).
[18] Hooper R., Macosko C. W., Derby J. J., *Chemical Engineering Science*, **55,** 5733 (2000).
[19] Yvonnet J., Ryckelynck D., Lorong P., Chinesta F., *International Journal for Numerical Methods in Engineering*, **60**, 1451 (2004).
[20] Alfaro I., Yvonnet J., Chinesta F., Cueto E., *International Journal for Numerical Methods in Engineering*, **71**, 1436 (2007).
[21] Dong L., Makradi A., Ahzi S., Remond Y., *Journal of Materials Processing Technology*, **209**, 700 (2009).
[22] Defauchy D., *27th Annual Meeting of the Polymer Processing Society*, Marrakech, Marrocco (2011).